Original Paper

Facile synthesis of chromium chloride/poly(methyl methacrylate) core/shell nanocapsules by inverse miniemulsion evaporation method and application as delayed crosslinker in secondary oil recovery

Jing-Yang Pu [a, b, *], Keith P. Johnston [c, **], Ping-Keng Wu [c], Muaaz Ahmad [c], Ming-Liang Luo [a, b], Na Zhang [d], Ju-Tao He [e]

[a] School of Petroleum Engineering, China University of Petroleum (East China), Qingdao, 266580, Shandong, China
[b] Key Laboratory of Unconventional Oil & Gas Development (China University of Petroleum (East China)), Ministry of Education, Qingdao, 266580, Shandong, China
[c] Mcketta Department of Chemical Engineering, The University of Texas at Austin, Austin, TX, 78712, USA
[d] Department of Energy and Mining Engineering, Shandong University of Science and Technology, Qingdao, 266590, Shandong, China
[e] No. 7 Oil Production Plant of PetroChina Changqing Oilfield Branch, Qingyang, 745100, Gansu, China

ARTICLE INFO

ABSTRACT

Cr(III)−hydrolyzed polyacrylamide (HPAM) gels have been extensively studied as a promising strategy controlling waste water production for mature oilfields. However, the gelation time of the current technologies is not long enough for in-depth placement. In this study, we report a novel synthesis method to obtain chromium chloride/poly(methyl methacrylate) (PMMA) nanocapsules which can significantly delay the gelation of HPAM through encapsulating the chromium chloride crosslinker. The chromium chloride-loaded nanocapsules (Cr−NC) are prepared via a facile inverse miniemulsion evaporation method during which the hydrophobic PMMA polymers, pre-dispersed in an organic solvent, were carefully controlled to precipitate onto stable aqueous miniemulsion droplets. The stable aqueous nanodroplets (W) containing Cr(III) are dispersed in a mixture of organic solvent (O_1) with PMMA and nonsolvent medium (O_2) to prepare an inverse miniemulsion. With the evaporation of the O_1, PMMA forms Cr−NCs around the aqueous droplets. The Cr−NCs are readily transferred into water from the organic nonsolvent phase. The Cr−NCs exhibit the tunable size (358−983 nm), Cr loading (7.1%−19.1%), and Cr entrapment efficiency (11.7%−80.2%), with tunable zeta potentials in different PVA solutions. The Cr−NCs can delay release of Cr(III) and prolong the gelation time of HPAM up to 27 days.

1. Introduction

Excessive water production in secondary oil recovery operations is a major problem encountered in most mature oil fields (Reddy et al., 2002; Seright and Brattekas, 2021; Sydansk and Southwell, 2000). Placing a blocking agent deep into the reservoir to block highly permeable channels or fractures and divert water flow into unswept productive zones would be desirable to improve sweep efficiency. Cr(III)-polyacrylamide gel is commonly applied as an effective blocking agent because of its advantages of controllable gelation time, adjustable strength, and good injectivity (Sun et al., 2018). During placement, a polymer solution mixed with Cr(III) crosslinkers is injected into formations to allow gelation to occur (Willhite and Pancake, 2004). Currently, chromium acetate is widely used to delay gelation by decelerating the interaction between Cr(III) and carboxyl groups of Cr(III)−hydrolyzed polyacrylamide (HPAM) gel system (Moradi-Araghi et al., 1988). However, the typical gelation time for Cr(III)−ligand complexes is still in the order of a few hours to several days (Willhite and Pancake, 2004). In addition, for in-depth placement, the unpredictable loss of ligands from Cr(III)−ligand complexes due to shear degradation and contact with reservoir minerals and fluids create

* Corresponding author. School of Petroleum Engineering, China University of Petroleum (East China), Qingdao, 266580, Shandong, China.
** Corresponding author.
E-mail addresses: 20200099@upc.edu.cn (J.-Y. Pu), kpj@che.utexas.edu (K.P. Johnston).

uncertainty in the gelation profile (Khamees and Flori, 2018).

For in-depth fracture blocking projects, a controlled release delivery system of entrapped Cr(III) that may delay the gelation of HPAM for periods in the order of a month is greatly needed. Large particles, such as microspheres, may settle out of solutions or impede penetration into reservoir rocks due to size-exclusion effects (Cordova et al., 2008). Therefore, millimeter-sized particles have already shown potential delayed Cr(III) release properties in field applications in our previous studies (Pu et al., 2019a, 2019b). Several polymeric materials in the forms of nanoparticles, polyelectrolyte complexes, microcapsules, and nanocapsules (NCs) are of interest for delaying release of crosslinkers (Musyanovych and Landfester, 2014; Ogolo et al., 2012). For example, Guan et al. studied a nanogel that can hold the metallic ion crosslinker Cr(III) and presents colloidal stability to impede agglomeration. The nanogel helps protect Cr(III) during transport in the formation and exhibits delayed Cr(III) release due to polymer degradation (Guan et al., 2017). Cordova et al. found that nanoparticle polyelectrolyte complexes are effective for entrapping and delivering small molecules like Cr(III) (Cordova et al., 2008). However, polyelectrolyte complexes may degrade upon exposure to monovalent or multivalent ions, such as KCl, thus resulting in the premature release of crosslinkers (Gao et al., 2015; Veisi et al., 2018).

Nanocapsules (NCs) or nanometer-sized hollow spheres with thin shells have been widely used as effective drug delivery devices for controlled release purposes (Paiphansiri et al., 2006b). The term "controlled release" includes a range of different release profiles and mechanisms, such as targeted, triggered, or sustained (or extended) release. The available payload volumes of NCs are higher than those of nanoparticle matrixes and polyelectrolyte complexes. NCs may be templated through commonly utilized microemulsion or miniemulsion techniques, such as emulsification solvent evaporation (Fickert et al., 2016; Yin et al., 2007), double emulsion solvent evaporation (W/O/W-E) (Iqbal et al., 2015), and emulsification solvent diffusion (Alvarez-Román et al., 2001; Piñón-Segundo et al., 2018). The microemulsion or miniemulsion technique is known to be a versatile tool for preparing polymer NCs with either an oily or an aqueous core (Crespy et al., 2007). The sizes of the droplets of the dispersed phase in microemulsions are less than 200 nm and are usually 10—140 nm (Eastoe et al., 2013). Miniemulsions are kinetically stable systems in which dispersed droplets with a size range of 50—500 nm are formed by a high shear force applied on a system containing a mixture of two immiscible liquids with a certain amount of surfactant (Koppel, 1972). Currently, W/O/W-E approach have been developed for controlling release of various payloads in fields of food and medicine. However, the entrapment efficiency of the payloads is usually low due to the leakage occurred between the two water phases.

The objective of this study is to prepare nanocapsules (Cr—NCs) that contain high levels of Cr(III) through a water/oil miniemulsion solvent evaporation (W/O-E) process (Paiphansiri et al., 2006b). The aqueous nanodroplets containing $CrCl_3$ were stabilized by Span80 emulsifier in an oily mixture of dichloromethane (DCM, O_1) and cyclohexane (cycC6, O_2) (Landfester, 2009). A polymethyl methylacrylate (PMMA) polymeric shell was formed upon the evaporation of the PMMA solvent DCM, whereas cyclohexane (cycC6), the nonsolvent, was retained in the oily mixture (Néstor et al., 2011). The stability of W/O miniemulsion was optimized via tunning the ratio of Span80 and W phase. It was found that, the W/O-E approach demonstrated significantly high Cr(III) loading and Cr(III) entrapment efficiency, compared with conventional W/O/W double emulsion approach by replacing the outer water phase with non-solvent oil phase. In addition, a sample centrifugation-based transfer method was developed for preparing the Cr—NC dispersion. The sizes of Cr—NCs were dependent on Span80/W ratio and PMMA feed amount. The transferred Cr—NCs showed stable dispersibility in PVA solution with accordingly pH. The Cr—NCs showed controllable Cr(III)-release capability, resulting in delaying gelation of HPAM polymer up to 27 days. The Cr—NC/HPAM gel system demonstrated potential application in in-depth gel treatment field of secondary oil recovery.

2. Experimental

2.1. Materials

Chromium chloride ($CrCl_3 \cdot 6H_2O$, $M_w = 266.45$ Da), PMMA ($M_w = 120$ kDa and 15 kDa), poly(vinyl alcohol) (PVA, $M_w = 13$—23 kDa), HPAM ($M_w = 520$ kDa, hydrolysis degree: ~20%), sorbitan mono-oleate (Span80, $M_w = 428.6$, HLB: 4.2), Tween40, DCM, and cycC6 (anhydrous, 99.5%) were purchased from Sigma and used without further purification. HCl (1 mol/L), HNO_3 (2 mol/L), and NaOH (0.5 mol/L) were obtained from Fisher Scientific.

AEC brine formula: 18.3 mmol/L $CaCl_2$ + 0.5 mol/L NaCl + 0.15 mol/L $NaHCO_3$.

2.2. Preparation of Cr—NCs through the W/O-E approach

The procedure for the formation of Cr—NCs was modified from a previously reported process (Paiphansiri et al., 2006b). A typical process for Cr—NC preparation was as follows: $CrCl_3$ (water phase (W)) solution was first prepared by dissolving $CrCl_3 \cdot 6H_2O$ in deionized water (DIW) (300—460 mg/mL). The pH was adjusted with 40 wt% NaOH to 2.4. The organic continuous phase comprising DCM (10 mL, oil phase (O_1)), PMMA (200 mg), and Span80 (0.1—0.5 g) was prepared in a 40 mL glass vial. The W phase was added into O_1 with the addition of a certain volume of cycC6 (15 mL, oil phase (O_2)) to prepare a W—O mixture. The mixture was emulsified for 120 s using an Ultra-Turax (12400 rpm) homogenizer. The emulsion was subsequently placed in an oil bath for incubation at 50 °C with a chosen stir rate (250 rpm) for 8 h to completely evaporated of DCM from the mixture. The final product volume was controlled at 10 mL.

2.3. Transfer of NCs into aqueous solutions and purification

The Cr—NCs (5 mL of native NC solution) were separated from cycC6 and Span80 via ultracentrifugation (Beckman) at 12,000 rpm for 30 min. The pellet was dried at room temperature for 30 min before being redispersed in 1% PVA solution (10 mL) with stirring at room temperature. The dispersion was centrifuged (12,000 rpm, 30 min) several times until its supernatant became clear. The supernatant was replaced with 1% PVA solution, and the pellet was redispersed each time.

2.4. Characterization

2.4.1. Size analysis of W/O-E miniemulsion

The droplet size of miniemulsions were measured at 25 °C through dynamic light scattering (DLS) using a Malvern Nano ZS (Malvern Instrument Ltd., US) (Koppel, 1972). In detail, 0.5 mL of the miniemulsion was mixed with 2 mL of cycC6 in a quartz cuvette for DLS measurements. The mean volume diameters of the droplets were determined. Scattered light was collected at 90° with an avalanche photodiode detector. All measurements were made over a period of 1 min and in quadruplicate, where the mean size (volume distribution) of the four runs was recorded. The FT-IR measurement was employed for detecting the PMMA shell and the results was shown in Fig. S1 in Supporting Information.

2.4.2. Size, zeta potential, and morphology analysis of Cr−NC

Cr−NC nanocapsules dispersed in PVA solution were separately analyzed by DLS to determine their size distribution and zeta potential at 25 °C. The samples were diluted by a factor of 100 in DIW, AEC brine, or different concentrations of PVA solutions. Size distribution data was directly imported from the Malvern Zetasizer software.

The dispersions were dried in vacuo at room temperature to investigate the morphology of the NCs using an environmental scanning electron microscope (ESEM, Quanta 650). In ESEM, electrons are accelerated to the energy of 20 keV and are converged by electromagnetic lenses to the surface of the sample. The dried Cr−NCs were mounted on carbon-coated grids before coating with Au to avoid degradation.

2.4.3. Cr(III) loading and entrapment efficiency determination

The solid content of the capsules in the final dispersion was determined gravimetrically. A known volume of the dispersion was dried at 120 °C overnight, and the final weight of the dry solid was determined. For the determination of the final Cr(III) fraction in the NCs, 1 mL of the dispersion was mixed with 2 mL of 2 mol/L HNO_3 solution and 2 mL of 2 mol/L HCl solution in a Schlenk tube. The Schlenk tube was fitted with a condenser and placed in an oil bath that was preheated at 100 °C overnight with continuous reflux. The digested sample was then cooled down to room temperature and diluted for inductively coupled plasma−optical emission spectroscopy (ICP−OES). ICP−OES measurements were made in triplicate using a Varian 710 instrument, argon gas, 2 wt% HNO_3 solution, and 1.2 kW plasma. Digested samples were made by serially diluting 1 mol/L Cr(III) solution with 2 wt% HNO_3 solution. Cr(III) loading, which was the mass ratio between Cr(III) and the NCs, was calculated as follows:

$$\text{Cr loading} = \frac{C_{\text{Cr}(III),\text{final}}}{C_{\text{capsules,final}}} \times 100\%$$

where $C_{\text{Cr}(III),\text{final}}$ is the final entrapped concentration of Cr(III) in the dispersion; and $C_{\text{capsules,final}}$ is the final concentration of capsules in the dispersion. The entrapment efficiency (E_E) of the NCs was evaluated as follows:

$$E_E = \frac{m_{\text{Cr(III),final}}}{m_{\text{Cr(III),feed}}} \times 100\%$$

where $m_{\text{Cr(III),final}}$ is the final entrapped mass of Cr(III) in the dispersion; and $m_{\text{Cr(III),feed}}$ is the feed mass of Cr(III). The detailed calculation of the nanocapsule basis was provided in Section. S2 in Supporting Information.

2.4.4. Cr(III) release analysis

A membrane dialysis technique was used to measure the release rate of Cr(III) from the Cr−NCs in accordance with a previous study (Cordova et al., 2008). A dialysis bag was prepared by sealing two ends of membrane tubing (Standard RC Tubing, M_W of cut off: 6−8 kD). One end of the bag was sealed by using a weighted closure to stabilize the bag during stirring. A known concentration of Cr−NC (PMMA-257-Cr) dispersion ($C_{\text{Cr(III)}} = 1$ mg/mL) was added to the 1±0.05 mL dialysis bag. The dialysis bag was permeable to water and Cr(III) but not PMMA. The bag was placed in 200 mL of AEC brine solution, which was used as the dialysate. The dialysis bag was stirred at 200 rpm in water at 50 °C for 200 days. 2 mL of buffer was taken from the dialysate at different periods for ICP−OES. A total of 1 mL of CrCl$_3$ standard solution ($C_{\text{Cr(III)}} = 1$ mg/mL) was used as the control. The shear resistance property of Cr−NC has

been tested using a blender and the results has been demonstrated in Fig. S2 in Supporting Information.

2.4.5. Delayed crosslinking HPAM test

HPAM stock solution (20,000 ppm) was prepared by dissolving solid HPAM in AEC brine and stirring vigorously for 10 h. The HPAM stock solution was mixed with AEC brine and then with the purified NC dispersion. The amount of each component was adjusted such that the final gelant contained 20,000 ppm HPAM, and a known amount of Cr(III) (300−600 ppm) was present in the AEC brine solution. Some gelant samples were added with 0.5 mol/L HCl or 0.5 mol/L NaOH to produce the desired pH. The gelant was vortexed for 1 min before incubation in a 50 °C oven. Gelation was determined on the basis of viscosity changes by using a Brookfield digital viscometer (Model DE-I) with a CPA-44YZ cup and CPA 40Z spindle at 25 °C. The gel time was defined as the time when the viscosity of the gelant increased abruptly to >1028 cP (limit of the viscometer) at the shear rate of 2.25 s^{-1}. An entire sample preparation procedure was provided in Section S4 in Supporting Information.

3. Results and discussion

3.1. Stability of W/O miniemuslion

3.1.1. Effect of Span80 on miniemulsion droplet stability in cycC6 and the DCM−cycC6 mixture

The emulsion stability of W/O (water−Span80−cycC6) was studied by monitoring droplet size as the function of emulsification time with varying Span80 concentrations (Span80/W, with the water weight held constant) in the mixture. An appropriate surfactant can prevent coalescence by stabilizing droplets either electrostatically or sterically. The results showed that the initial droplet size decreased from 796 to 219 nm when the Span80 ratio was increased from 10% to 100% (Fig. 1a). The final droplet sizes of the emulsions after 16 h of emulsification ranged from 256 to 207 nm. These sizes were all at the droplet level of the miniemulsion series. Moreover, they revealed that the minimum Span80 concentration needed to form the complete emulsion with stable 200 nm droplets was 20% Span80/W. The rapid coalescence of the emulsion with the 10% Span80/W sample emulsion resulted in a large initial size (796 nm). Except that, the samples with 20%, 40%, and 100% Span80/W had ~200 nm aqueous droplets with relatively constant sizes for 16 h.

The minimum concentration of Span80 required to form a homogenous emulsion was studied by measuring the droplet size at different evaporation periods to investigate the emulsion stability of the aqueous−DCM−cycC6 system, which was the actual system used for the preparation of NCs. Fig. 1b shows the change in droplet size as a function of evaporation time. Although the sizes of both samples with different Span80/W concentrations increased with time, the 100% Span80/W sample showed a considerably smaller size (720.9 nm) after 16 h than the 20% Span80/W sample (2000 nm). This result matched the Cr−NC size of the 100% Span80/W sample (983 nm) shown in Table 1. The ability of the Span80 to stabilize reverse miniemulsions with small droplet sizes was essential for templating the NCs. Given that Span80 is nonionic, it is less likely to be influenced by Cr(III) than by nonionic surfactants.

3.1.2. Formation schematic of Cr−NC

Nanocapsules were synthesized according to the procedure shown in Fig. 2. In principle, the NCs were formed by controlling precipitation of polymers from the continuous phase onto the interface of small and stable water droplets upon the evaporation of the solvent DCM in presence of the nonsolvent cycC6. Theoretically, no DCM residue should remain in the cycC6 phase after the
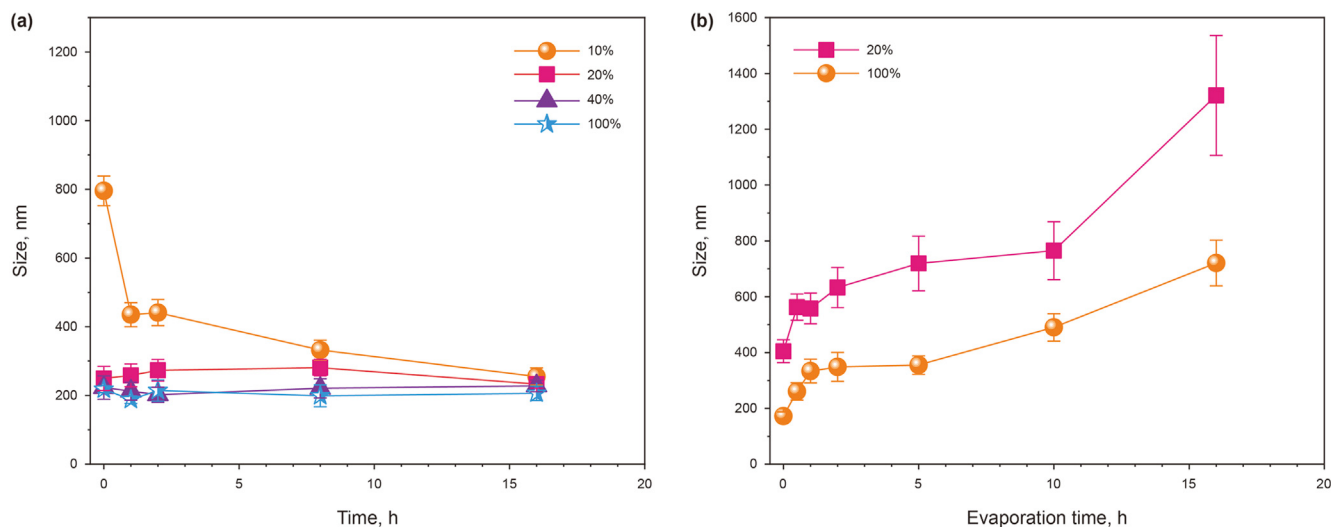
Fig. 1. Hydrodynamic diameter of 0.5 mL of aqueous droplets in 15 mL of cycC6 emulsified by Span80 as a function of time at 50 °C in the absence (**a**) or presence (**b**) of 10 mL of DCM (containing 200 mg PMMA).

Table 1
Sizes of Cr−NCs measured by DLS (120 kDa PMMA, Cr(III) feed of 78 mg/mL, and 1% PVA).

Sample name	PMMA, mg	Span80/W, %	Cr−NCs dispersed in DIW		Cr−NCs dispersed in AEC brine	
			Size[a], nm	PI[b]	Size[a], nm	PI[b]
NC-1	200	20	358	0.21	351	0.19
NC-2	200	50	768	0.19	690	0.20
NC-3	200	100	983	0.22	935	0.21
NC-4	200	150	502	0.22	498	0.22
NC-5	200	200	487	0.27	483	0.29
NC-6	100	50	560	0.17	572	0.25
NC-7	300	50	633	0.19	689	0.21

Notes: [a] Hydrodynamic radii of Cr−NCs dispersed in DIW and AEC brine were determined at 90°; [b] Polydispersity index.

evaporation of the miniemulsions at 50 °C for more than 8 h. The precipitation and deposition of part of PMMA on the surfaces of the nanodroplets are illustrated in Fig. 2a. In addition, some of the PMMA precipitated in the oil phase and formed a coagulated ball that settled to the bottom of the vessel during evaporation. The maximum initial volume ratio of cycC6 to DCM that was needed to dissolve the required amount of PMMA completely was 1.5:1 (Fig. S3). An aqueous solution of CrCl₃ was emulsified to obtain small and stable droplets with an initial size of approximately 200 nm. In addition, the dissolved Cr(III) acted as the lipophobe that suppressed Ostwald ripening by increasing the osmotic pressure inside the nanodroplets (Paiphansiri et al., 2006a). Therefore, individual nanodroplets can be stabilized during evaporation.

3.1.3. Formation, transfer, and purification of Cr−NCs

Emulsion stability against settling or coalesces of droplets is one of the key factors for evaluating the interfacial properties of W/O emulsions. Fig. 2b shows the changes in turbidity and volume as a function of time after evaporation began. Upon stirring for over 7 h, the emulsions appeared turbid without the obvious coalescence of aqueous nanodroplets, indicating that stabilization with Span80 can stabilize emulsions within 7 h. In the original study that utilized this method, a block copolymer was used as the surfactant to stabilize water droplets and to direct PMMA to the interface (Muñoz-Espí and Landfester, 2020). Furthermore, the copolymer

adsorbed on the PMMA surface and provided steric stabilization in cycC6. Given the complexity of synthesizing the commercially unavailable block copolymer, we decided to synthesize Cr−NCs with the commonly used low-molecular-weight surfactant Span80, which is soluble in cycC6 with the low HLB of 4.2. Span80 is insoluble in water but contains a nonionic hydrophilic sorbitan headgroup. The hydrophobic tails of the alkane chain enable the steric stabilization of water miniemulsion droplets. Although Span80 did not provide as much steric stabilization as a block copolymer with considerably longer steric chains, it did stabilize a minor fraction of the resulting PMMA NCs in cycC6 (Capdevila et al., 2010; Davies et al., 1987). The Span80-to-water (Span80/W) ratio was varied to manipulate the NC properties. A PMMA coagulate was found at the end of the evaporation as shown in Fig. 2b. A minor part of PMMA formed NCs upon accumulating on the surfaces of the water droplets. This NC fraction could be redispersed by shaking to break up the NC aggregates. The equilibrium volume of the emulsion was determined by evaporation time and was controlled to 10 mL.

The transfer and purification procedures of the prepared Cr−NCs were depicted in Fig. 3a. In detail, cycC6 was removed through centrifugation at 12,000 rpm for 30 min. Then, the obtained pellet was redispersed in 1% PVA solution. After a secondary centrifugation cycle, a colored pellet was obtained at the bottom of the tube. This pellet was Cr(III)-entrapping Cr−NCs. These Cr−NCs were washed at least twice with 1% PVA to remove free Cr(III) to prevent premature gelation in subsequent tests. Washing was repeated if the supernatant remained colored after centrifugation. The final uniform homogeneous dispersion of Cr−NCs was obtained by adding 10 mL of 1% PVA under probe sonication (15% amplitude, 2 min). The products at different stages are shown in Fig. 3b.

3.2. Characterization of fabricated Cr−NC nanocapsules

3.2.1. Effect of Span80/W

The effects of various Span80 to water phase ratio (Span80/W) on the formation of Cr−NCs were investigated to determine the optimal preparation formula. The results were summarized in Table 1. The structures of the prepared Cr−NCs, which were spherical with continuous intact shells, were detected. None of the
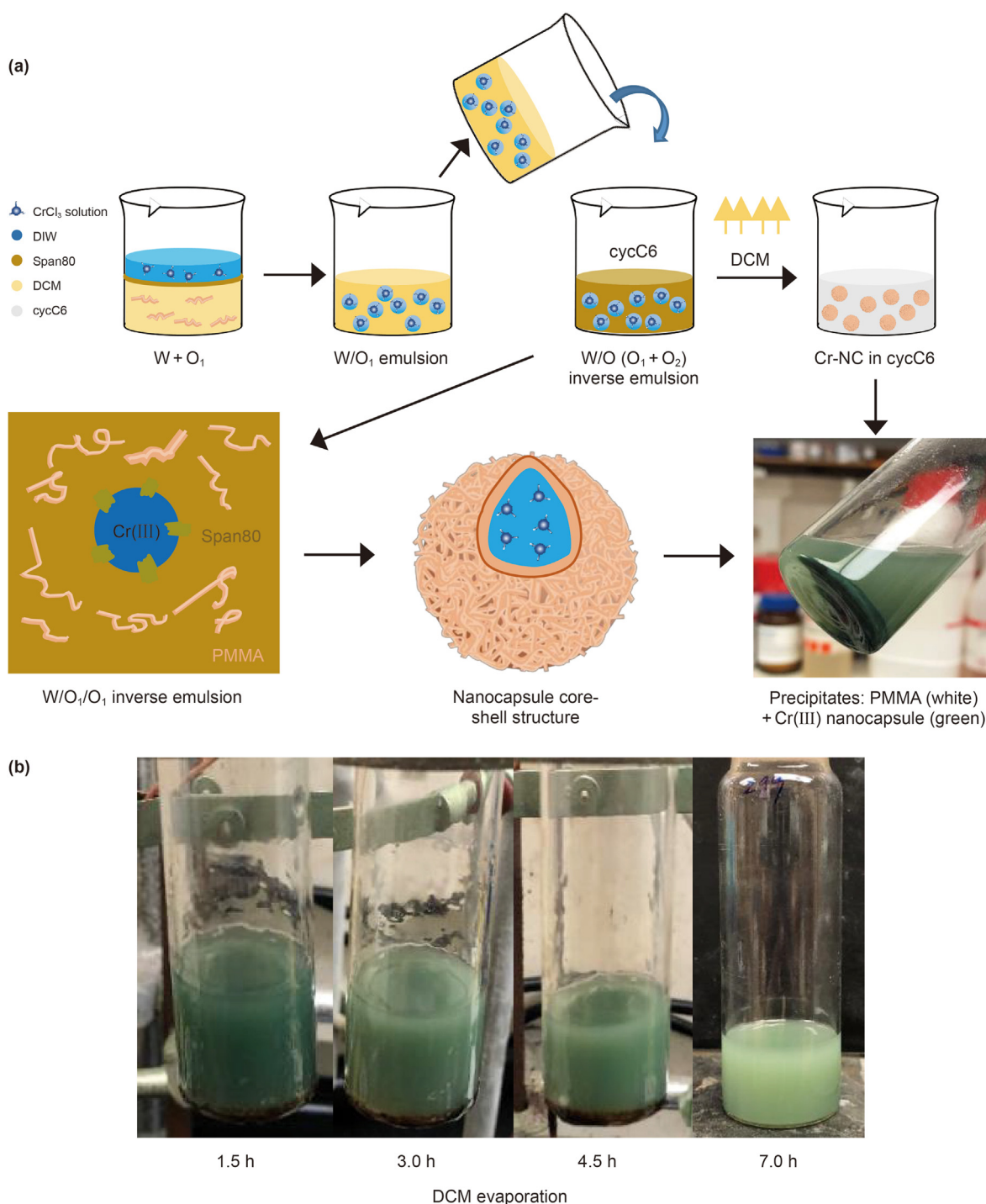
(a)

W + O₁ → W/O₁ emulsion → W/O (O₁ + O₂) inverse emulsion → DCM → Cr-NC in cycC6

W/O₁/O₁ inverse emulsion

Nanocapsule core-shell structure

Precipitates: PMMA (white) + Cr(III) nanocapsule (green)

(b)

1.5 h   3.0 h   4.5 h   7.0 h

DCM evaporation

Fig. 2. (**a**) Schematic of the mechanism of Cr—NC formation via the controlled nanoprecipitation of PMMA onto miniemulsion droplets containing Cr(III); (**b**) Pictures taken in different evaporation periods.

Cr—NCs ruptured during preparation. In addition, it was found that Span80/W ratio controlled the integrity, size, and zeta potential of Cr—NCs. For example, Fig. 4a-1 to a-5 shows the morphologies of the Cr—NCs using various ratio of Span80/W. In detail, small nanocapsules (358 nm, Fig. 4a-1) with high integrity were fabricated with 20% Span80/W, while the size increased to 768 nm (Fig. 4a-2) as the ratio of Span80/W was raised to 50%. Large nanocapsules with a wide distribution of nanocapsule sizes were obtained when the Span80/W ratio was increased to 100% (Fig. 4a-

3). Higher Span80/W ratio might increase the viscosity of the miniemulsion resulting in reducing the emulsion efficiency. The morphology of Cr—NCs were strongly affected by the viscosity increase of the miniemulsion when the Span80/W ratio was increased to 150%, resulting in the aggregation of the fabricated nanocapsules (Fig. 4a-4). As the Span80/W ratio increased to 200%, ellipsoid-like nanocapsules were synthesized which showed low quality of sphericity (Fig. 4a-5). The size distribution and zeta potential of the Cr—NCs dispersed in 1% PVA were exhibited in Fig. 4b.
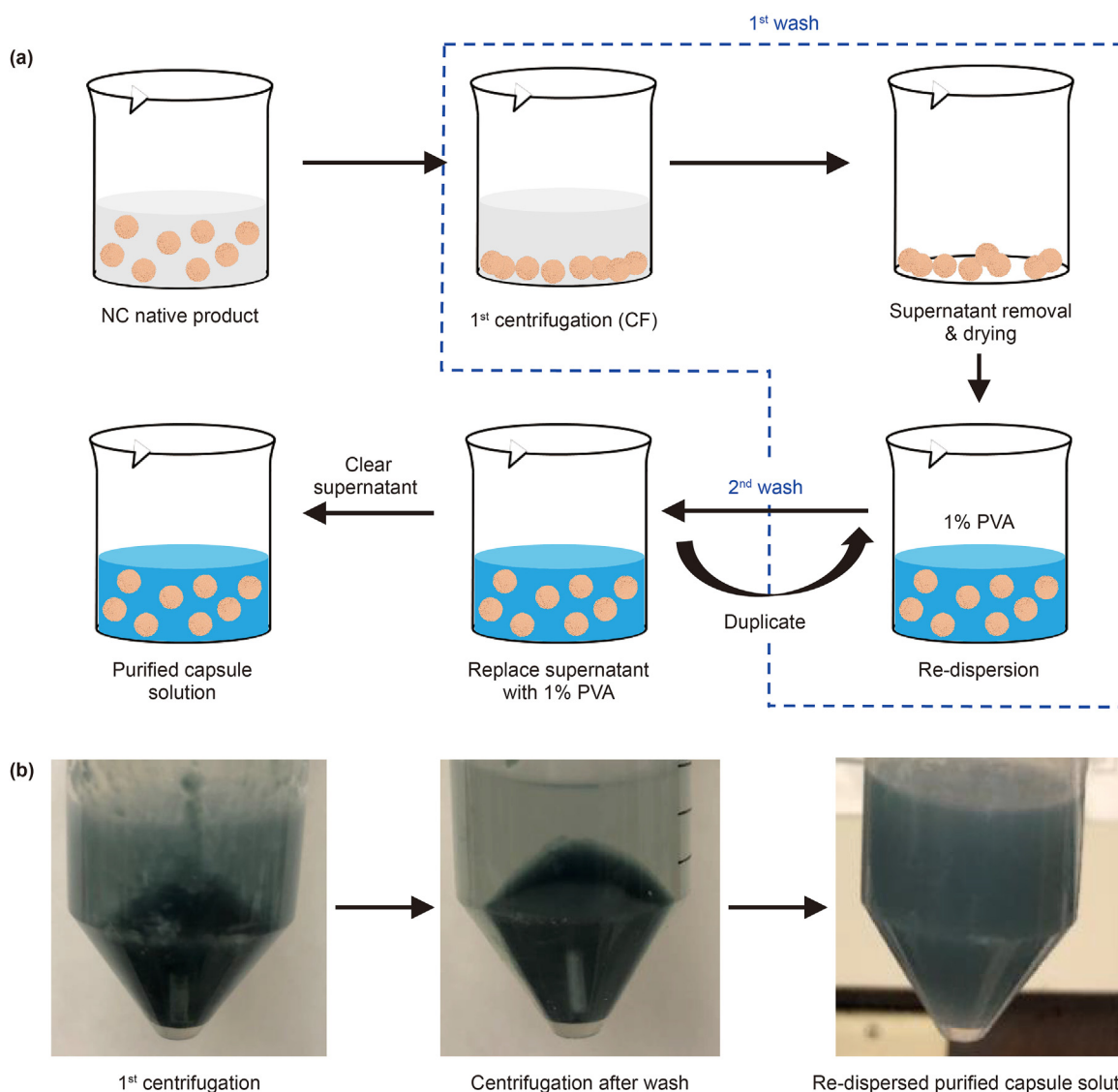
Fig. 3. (**a**) Transfer and purification of Cr−NCs (NC-2) from cycC6 to the aqueous PVA solution and (**b**) product in the first centrifugation stage, refill aqueous phase stage, and redispersed stage.

Both the largest size (983 nm) and lowest zeta potential (−34.9±3.4 mV) were found at the Span80/W ratio of 100%. The sizes of the Cr−NCs increased first from 358 to 983 nm as the Span80/W ratio was increased from 20% to 100%. At the Span80/W ratio higher than 100%, the sizes decreased down to 487 nm with increasing the concentration.

The solid contents of the 1% PVA dispersed samples are summarized in Table 2. The initial Cr(III) concentrations for all the samples were held constant at 39 mg for the comparison purpose. After the transfer, the final nanocapsule, [NC], in 1% PVA solution was between 10.1 and 18.5 mg/mL, which was less than the theoretical one (24.8 mg/mL, Section S2 in Supporting Information). It was found that Cr(III) loading increased up to 19.1% as the Span80/W ratio was increased from 20% to 100% and then decreased down to approximately 8%. The maximum Cr(III) loading (19.1%) was less than the theoretical value which was 19.3% as shown in Section S2 in Supporting Information. In addition, the highest Cr(III) entrapment efficiency of 80.2% was obtained at the Span80/W ratio of 50%. For the sample with only the Span80/W ratio of 20% and whose products were mixed PMMA aggregates and nanocapsules as mentioned previously, for which the Cr(III) loading was as low as

7.1%. The samples with 150% and 200% Span80/W ratios may increase the viscosity of the aqueous phase likely by forming Span80 vesicles (Hayashi et al., 2013). Consequently, the loadings of Cr(III) decreased under these conditions. High Span80/W ratios led to the formation of Span80 vesicles that reduced emulsion stability and caused PMMA to precipitate in the form of nanoparticles instead of forming Cr−NCs (Kato et al., 2008). As an alternative to the 120 kDa PMMA, 200 mg 15 kDa PMMA could also be applied to prepare nanocapsules (named as NC-L) with desirable sizes ranging from 247 to 626 nm with 100% and 200% Span80/W ratio, as shown in Table S2. Since the release profile of Cr(III) is controlled by the diffusion of the shell polymers, which is, in some extent, depended by the molecular weight of the polymers. Only 120 kDa PMMA was used in the further studies. The result of the mechanical shear resistance of the Cr−NCs also support using the 120 kDa PMMA.

3.2.2. Effect of PMMA

Comparing the samples prepared by the same Span80/W ratio, it was found that various PMMA content, i.e., 100, 200, and 300 mg, affected the nanocapsule size, zeta potential, and solid contents, as shown in Tables 1 and 2, and Fig. 4c. In particular, the size (from 560
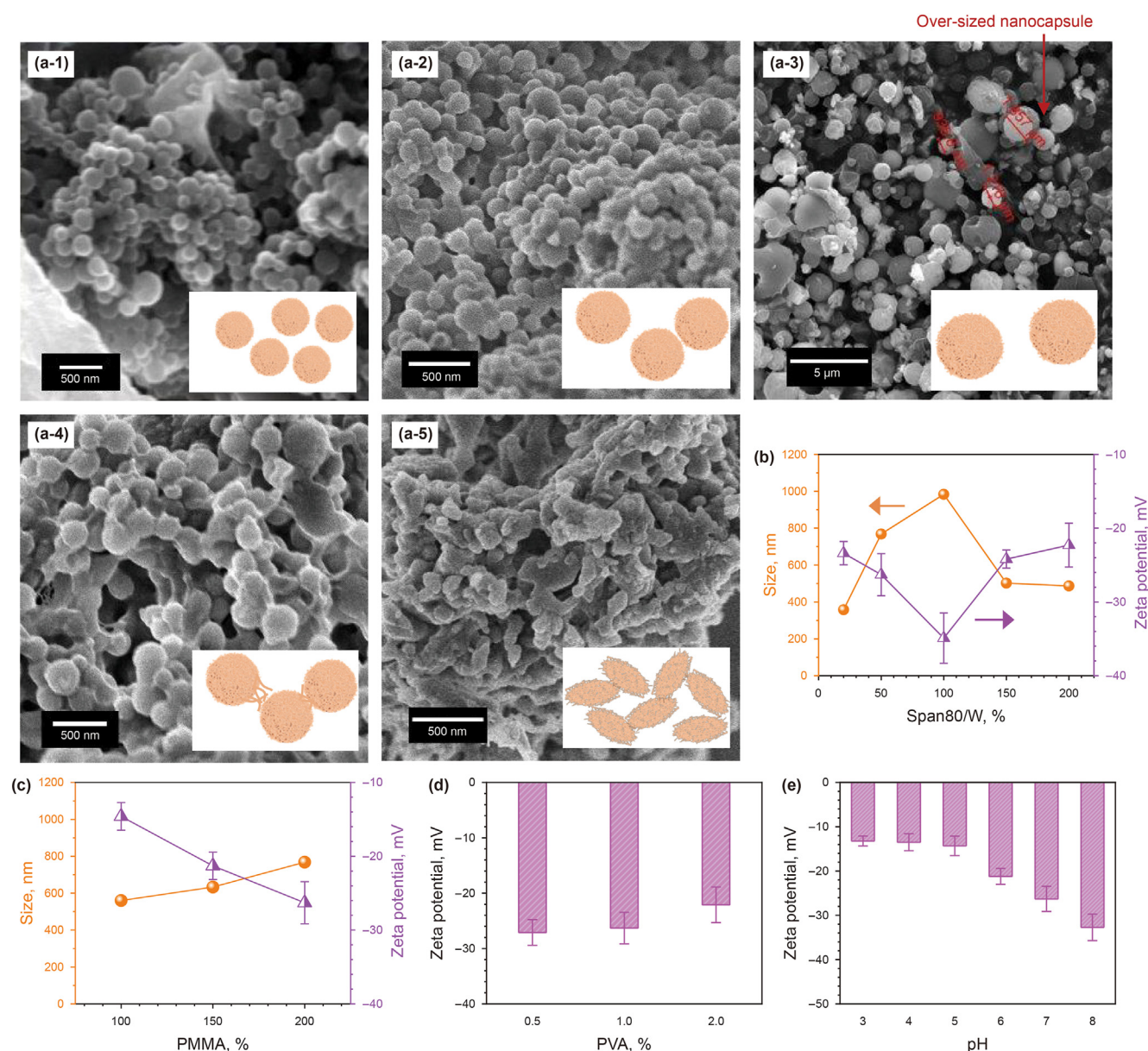
Fig. 4. SEM micrographs of the dried Cr–NCs with Span80/W ratios of 20%–200%: (**a-1**) 20%, (**a-2**) 50%, (**a-3**) 100%, (**a-4**) 150%, and (**a-5**) 200%. Effect of (**b**) Span80/W ratio, (**c**) PMMA concentration, (**d**) PVA stabilizer concentration, and (**e**) dispersion pH on sizes and zeta potentials of the fabricated Cr–NCs.

to 768 nm) and Cr(III) entrapment efficiency (from 38.2 to 80.2) were significantly increased as the increase of PMMA content from 100 to 200 mg, indicating that 100 mg was not sufficient for encapsulate all the water droplet. Comparing the samples prepared with 150 and 200 mg PMMA, it was found that the threshold of PMMA entrapment efficiency was obtained at the sample with 150 mg PMMA. The Cr(III) entrapment efficiency of the nanocapsules were significantly increased (from 38.2% to 80.2%) as the increase of PMMA amount (from 100 to 200 mg) as shown in Table 2. The results of zeta potential measurements demonstrated that the zeta potential of the samples reduced significantly from -14.6 ± 1.88 mV to -26.3 ± 2.85 mV as the increase of PMMA amount (from 100 to 200 mg).

3.2.3. Effect of PVA concentration and pH of dispersions

Fig. 4d shows the zeta potential versus the PVA concentration for samples with pH=7 and for different PVA concentrations. The

samples failed to be homogeneously dispersed in pure DIW after separated from the oil phase (cyclohexane). The zeta potential of nanocapsules increased from -27.1 ± 2.31 mV to -22.1 ± 3.21 mV as the PVA concentration increased from 0.5% to 2%. The adsorption of PVA, a nonionic surfactant polymer, onto nanocapsules neutralized the initially negative zeta potential. The neutralization ability of the nonionic surfactant to PMMA was not as strong as other anionic surfactant, i.e., SDS (Khademi et al., 2017).

To demonstrate the influence of the dispersion pH value, the zeta potential of the nanocapsule dispersion with pH ranging from 3 to 8 was measured and presented in Fig. 4e. The results showed that pH had more significant impact on the zeta potential of the dispersions when compared with PVA concentration. The equilibrium zeta potential of nanocapsule dispersion reduced from -13.2 ± 1.13 mV to -32.7 ± 2.99 mV as the pH value increased from 3 to 8. The zeta potential remained below zero at low pH referring to the existence of 1% PVA, which neutralized the change of PMMA pH value.
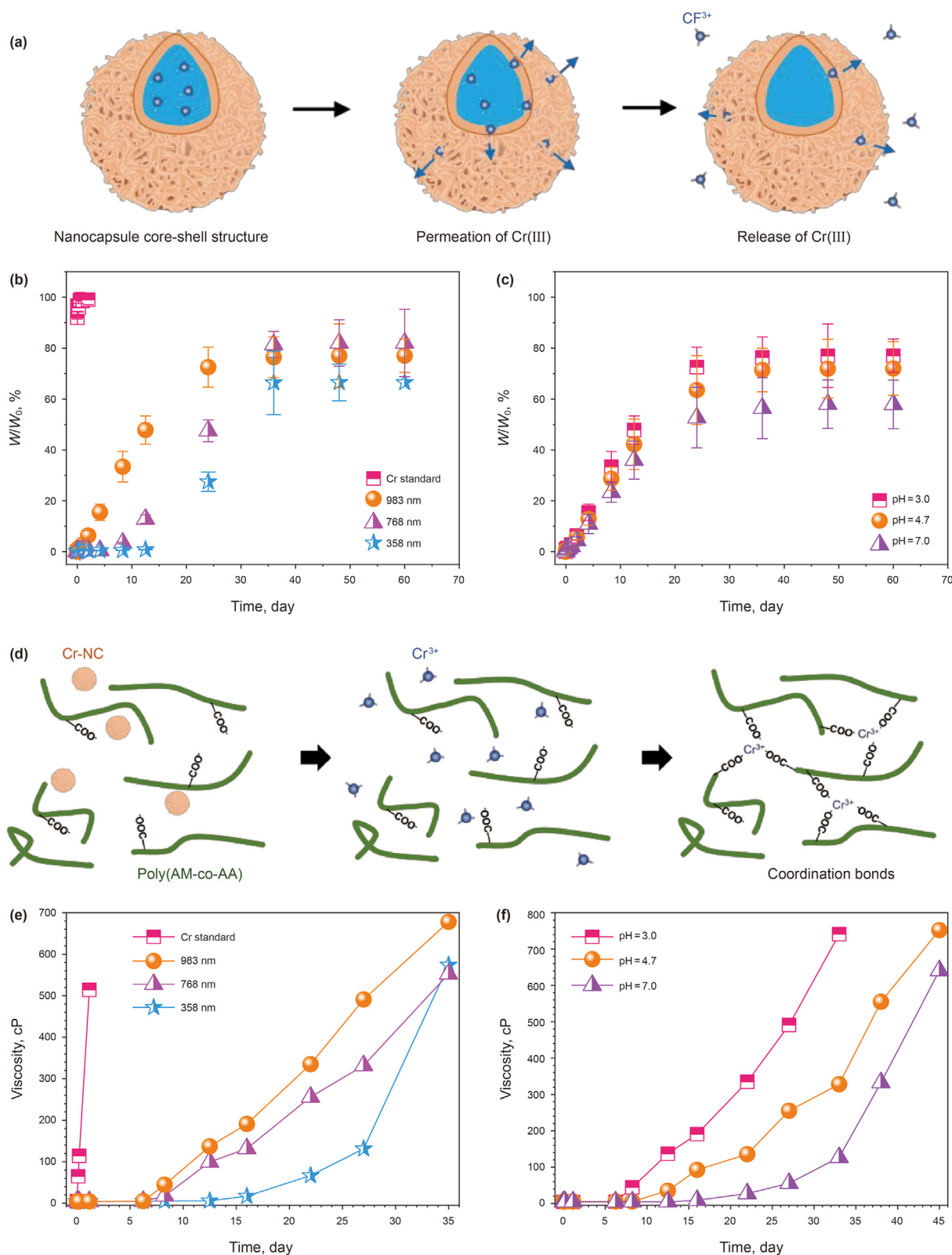
Fig. 5. (**a**) Schematic of Cr(III) release from the Cr−NC shells; (**b, c**) Dialysis result of NC-1 at 50 °C; (**d**) Schematic of HPAM gelation by Cr(III) released from NCs; (**e**) Gelation of 2% HPAM mixed with Cr−NCs of varying sizes (same final entrapped Cr(III) concentration in the mixture of 0.35 mg/mL) after the lag phase as determined on the basis of viscosity at pH=3; (**f**) Effect of pH value. Unless otherwise noted, the experiments used AEC-SW including 2% HPAM, and incubation at 50 °C.

Table 2

Characterization of Cr—NC nanocapsules prepared with different Span80/W ratios and PMMA amount (120 kDa PMMA and Cr(III) feed of 78 mg/mL).

Sample name	PMMA, mg	Span80/W, %	[NC][a], mg/mL	[Cr(III)][b], mg/mL	Cr(III) loading, %	Entrapment efficiency, %	
						Cr(III)	PMMA
NC-1	200	20	17.6	1.25	7.1	32.0	81.8
NC-2	200	50	18.5	3.13	16.9	80.2	76.9
NC-3	200	100	13	2.48	19.1	63.6	52.6
NC-4	200	150	14.1	0.46	7.4	11.7	68.2
NC-5	200	200	13.3	1.04	8.1	26.7	61.3
NC-6	100	50	10.1	1.49	14.8	38.2	86.1
NC-7	150	50	16.3	2.57	15.8	65.9	91.2

Notes: [a] [NC] = [PMMA for shell]+[encapsulated Cr(III)], final volume of dispersion is 10 mL; [b] Final Cr(III) means the ratio of encapsulated Cr(III) mass to the final dispersion volume.

3.3. Cr(III) release and delayed gelation characterization

3.3.1. Delayed release of Cr(III) from Cr—NCs

Previous works investigated three temperature-triggered methods (Esser-Kahn et al., 2011) for breaking Cr—NC shells: melting the shell wall in accordance with the polymer's melting temperature (T_m), inducing changes in porosity via polymer shrinkage (polymer diffusion), and thermo-mechanically degrading the shell wall. The shells of the Cr—NCs shell would not be expected to be broken at 50 °C because the glass transition temperature (T_g) of PMMA was approximately 100 °C as a result of its configuration and molecular weight. Therefore, Cr(III) was released in the second way by diffusing through the entangled PMMA shell as shown in Fig. 5a. Membrane bag dialysis was performed to examine Cr(III) release from Cr—NCs in AEC brine buffer. Cellulose membrane bags show high stability and electric neutrality and have been widely used in dialysis experiments on metallic ions. The membrane bag allows Cr(III) exchange between the inner and outer aqueous phases. The release capability of Cr(III) from Cr—NC was tested through the dialysis experiment.

The Cr(III) diffusion of the Cr—NCs with different sizes were conducted to prove the controlled release capacity of the Cr(III)-entrapping Cr—NC in AEC brine. The dialysis rate was investigated by drawing a curve of cumulative release ratio (W/W_0) vs. dialysis time, where W is the total dialyzed amount of Cr(III) and W_0 is the total initial amount of Cr(III). A chromium standard dialysis sample was separately prepared to showing the release rate differences between samples with or without encapsulation. It was found that the release behavior of Cr(III) was much slower than that of the unencapsulated CrCl$_3$ control sample at the same condition. The released W/W_0 ratio of the CrCl$_3$ standard sample reached approximately 100% in the first hour.

However, for all the Cr—NC samples, as shown in Fig. 5b, the W/W_0 ratio increased in first 30—35 h before reaching equilibrium. Cr—NC with 983 nm size released Cr(III) faster (20% in 5 h), than Cr—NCs with 768 nm size (13.5 h) or 358 nm size (16.2 h). the release rate, which is presented in Fig. 5b and c as the slope of the dialysis curve, is determined by two factors, surface area dominated polymer diffusion and the shell thickness. The shell thickness has not been discussed in this study but will be examined in further research. Instead, the PMMA entrapment efficiency was employed to reflect the thickness of the Cr—NCs. The samples with 983 nm size had the lowest PMMA entrapment efficiency (52.6%, as shown in Table 2) and the biggest size, resulting in thinner shell. Therefore, the sample with 983 nm size had the fastest Cr(III) release rate, compared with other two samples. On the contrary, the samples with 358 nm size had highest entrapment efficiency (81.8%) and smallest size, resulting in slowest release rate, as shown in Fig. 5b. The pH effect on the release kinetics of the Cr—NCs were investigated to study the release rate and final W/W_0 ratio as shown in

Fig. 5c. The results showed that the release rate of Cr(III) increased as the pH of the environmental aqueous phase decreased from 7 to 3, indicating that low pH accelerated the diffusion of PMMA polymer and the exchange rate of Cr(III). In addition, the final W/W_0 ratio of the dialyzed Cr(III) increased from 58% to 77% as the pH decreased from 7 to 3. The results showed that more entrapped Cr(III) remained in the nanocapsules with smaller size.

3.3.2. Effect of Cr—NC size on gelation time

The schematic of Cr(III) release and form bond with carboxyl group of HPAM polymers are demonstrated in Fig. 5d. The Cr(III) can form a coordination complex with the carboxyl group on the side chain of HPAM. The effects of nanocapsule size and environmental pH on the gelation time were investigated by separately mixing Cr—NCs with 2% HPAM. As shown in Fig. 5e, a CrCl$_3$ standard sample mixed with 2% HPAM as the control sample to prove the gelation capability of the CrCl$_3$. By contrast, the CrCl$_3$/HPAM control system without NCs gelled in 3 h at 50 °C. For all Cr—NCs with various sizes, the durations of the lag phases (Cr—NC/HPAM) without an increase in viscosity were approximately the same (6 days), indicating that the PMMA shells of all the Cr—NCs were intact. The gelation time of Cr—NC/HPAM samples increased from 6 to 13 days as the sizes of NCs decreased from 983 to 358 nm. The smaller Cr—NCs had higher PMMA entrapment efficiency than larger ones were suggestive of high actual thicker PMMA shell, which significant delayed the release rate of Cr(III).
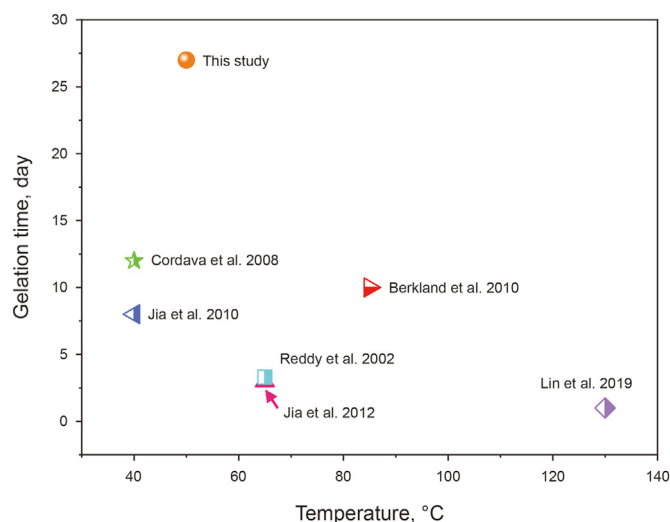

Fig. 6. Gelation time comparison at different temperatures (Cordova et al., 2008; Jia et al., 2010, 2012; Reddy et al., 2002; Berkland et al., 2010; Lin et al., 2019).

3.3.3. Effect of gelant pH on gelation time

The pH of the aqueous phase outside of the Cr−NCs influences the release of the Cr(III) by degrading of the PMMA polymer via hydrolysis. The lag phase was investigated at three different environmental pH values (3, 4.7, and 7) to further understand the release behavior of Cr(III). The solutions included 2% HPAM and 0.19% Cr−NC, which translated into 0.35 mg/mL (3.5%) entrapped Cr(III) (Fig. 5f). At pH = 7, the viscosity of the HPAM solution did not change over 27 days, indicating the presence of stable polymers with intact shells and negligible Cr(III) permeability. As the pH decreased, the gelation time increased significantly. At pH = 4.7, the viscosity steadily increased after a 12.5-day lag. At pH = 3, the crosslinking time decreased to 6 days, and then the fastest rate of viscosity increase was observed. These results were consistent with the acid-catalyzed hydrolysis of PMMA that led to shells with increased permeability. Compared with other previous HPAM gel studies whose gelation time are longer than 3 days, Cr−NC/HPAM gels showed a significant prolonged gelation time as shown in Fig. 6.

4. Conclusion

Cr−NCs with aqueous cores containing Cr(III) crosslinkers were fabricated by controlling the nanoprecipitation of PMMA onto inverse miniemulsion droplets in a W/O miniemulsion. Finely dispersed Cr−NCs were obtained after transferred to 1% PVA solution. The sizes of the nanocapsules were controlled between 358 and 983 nm depending on the Span80/W ratio and PMMA. The formed Cr(III)-entrapping NCs showed high Cr(III) loading of up to 19.1% and entrapment efficiency of up to 80.2%. By tunning the basis of the nanocapsules, the gelation time of HPAM could be controlled from 6 to 27 days in accordance with Cr−NC size and environmental pH. Large sizes and low pH led to the earlier release of Cr(III), resulting in fast gelation of HPAM.

Declaration of competing interest

The authors declare that they have no known competing financial interests or personal relationships that could have appeared to influence the work reported in this paper.

Appendix A. Supplementary data

Supplementary data to this article can be found online at https://doi.org/10.1016/j.petsci.2022.09.031.

References

Alvarez-Román, R., Barré, G., Guy, R.H., Fessi, H., 2001. Biodegradable polymer nanocapsules containing a sunscreen agent: preparation and photoprotection. Eur. J. Pharm. Biopharm. 52 (2), 191–195. https://doi.org/10.1016/S0939-6411(01)00188-6.

Berkland, C., Cordova, M., Liang, J.-T., Willhite, G., 2010. Polyelectrolyte Complexes for Oil and Gas Applications. US Patent. US2010/0056399A1.

Capdevila, M., Maestro, A., Porras, M., Gutiérrez, J.M., 2010. Preparation of Span 80/oil/water highly concentrated emulsions: influence of composition and formation variables and scale-up. J. Colloid Interface Sci. 345 (1), 27–33. https://doi.org/10.1016/j.jcis.2010.01.045.

Cordova, M., Cheng, M., Trejo, J., Johnson, S.J., Willhite, G.P., Liang, J.-T., Berkland, C., 2008. Delayed HPAM gelation via transient sequestration of chromium in polyelectrolyte complex nanoparticles. Macromolecules 41 (12), 4398–4404. https://doi.org/10.1021/ma800211d.

Crespy, D., Stark, M., Hoffmann-Richter, C., Ziener, U., Landfester, K., 2007. Polymeric nanoreactors for hydrophilic reagents synthesized by interfacial polycondensation on miniemulsion droplets. Macromolecules 40 (9), 3122–3135. https://doi.org/10.1021/ma0621932.

Davies, R., Graham, D.E., Vincent, B., 1987. Water−cyclohexane-"Span 80"−"Tween 80" systems: solution properties and water/oil emulsion formation. J. Colloid Interface Sci. 116 (1), 88–99. https://doi.org/10.1016/0021-9797(87)90101-9.

Eastoe, J., Hatzopoulos, M.H., Tabor, R., 2013. Microemulsions. In: Tadros, T. (Ed.), Encyclopedia of Colloid and Interface Science. Springer Berlin Heidelberg, Berlin, Heidelberg, pp. 688–729.

Esser-Kahn, A.P., Odom, S.A., Sottos, N.R., White, S.R., Moore, J.S., 2011. Triggered release from polymer capsules. Macromolecules 44 (14), 5539–5553. https://doi.org/10.1021/ma201014n.

Fickert, J., Landfester, K., Crespy, D., 2016. pH-responsive nanocapsules from silylated copolymers. Polym. Chem. 7 (26), 4330–4333. https://doi.org/10.1039/C6PY00878J.

Gao, Y., Chowdhury, M.R., Liang, J.T., Dhar, P., 2015. Effects of monovalent and multivalent ions on the stability of a polyelectrolyte complex with entrapped surfactants. J. Appl. Polym. Sci. 132 (25), 42099. https://doi.org/10.1002/app.42099.

Guan, H., Berkland, C., Moradi-Araghi, A., Liang, J.-T., Christian, T.M., Needham, R.B., Cheng, M., Scully, F.L., Hedges, J.H., 2017. Nanogels for Delayed Gelation. US Patent. US9796909B2.

Hayashi, K., Tatsui, T., Shimanouchi, T., Umakoshi, H., 2013. Membrane interaction between Span 80 vesicle and phospholipid vesicle (liposome): Span 80 vesicle can perturb and hemifuse with liposomal membrane. Colloids Surf. B Biointerfaces 106, 258–264. https://doi.org/10.1016/j.colsurfb.2012.12.022.

Iqbal, M., Zafar, N., Fessi, H., Elaissari, A., 2015. Double emulsion solvent evaporation techniques used for drug encapsulation. Int. J. Pharm. 496 (2), 173–190. https://doi.org/10.1016/j.ijpharm.2015.10.057.

Jia, H., Pu, W.-F., Zhao, J.-Z., Jin, F.-Y., 2010. Research on the gelation performance of low toxic PEI cross-Linking PHPAM gel systems as water shutoff agents in low temperature reservoirs. Ind. Eng. Chem. Res. 49 (20), 9618–9624. https://doi.org/10.1021/ie100888q.

Jia, H., Zhao, J.-Z., Jin, F.-Y., Pu, W.-F., Li, M.-Y., Li, K.-X., Li, J.-M., 2012. New insights into the gelation behavior of polyethyleneimine cross-linking partially hydrolyzed polyacrylamide gels. Ind. Eng. Chem. Res. 51 (38), 12155–12166. https://doi.org/10.1021/ie301818f.

Kato, K., Walde, P., Koine, N., Ichikawa, S., Ishikawa, T., Nagahama, R., Ishihara, T., Tsujii, T., Shudou, M., Omokawa, Y., Kuroiwa, T., 2008. Temperature-sensitive nonionic vesicles prepared from Span 80 (Sorbitan monooleate). Langmuir 24 (19), 10762–10770. https://doi.org/10.1021/la801581f.

Khademi, M., Wang, W., Reitinger, W., Barz, D.P.J., 2017. Zeta potential of poly(-methyl methacrylate) (PMMA) in contact with aqueous electrolyte-surfactant solutions. Langmuir 33 (40), 10473–10482. https://doi.org/10.1021/acs.langmuir.7b02487.

Khamees, T.K., Flori, R.E., 2018. A comprehensive evaluation of the parameters that affect the performance of in-situ gelation system. Fuel 225, 140–160. https://doi.org/10.1016/j.fuel.2018.03.115.

Koppel, D.E., 1972. Analysis of macromolecular polydispersity in intensity correlation spectroscopy: the method of cumulants. J. Chem. Phys. 57 (11), 4814–4820. https://doi.org/10.1063/1.1678153.

Landfester, K., 2009. Miniemulsion polymerization and the structure of polymer and hybrid nanoparticles. Angew. Chem. Int. Ed. 48 (25), 4488–4507. https://doi.org/10.1002/anie.200900723.

Lin, Y.-Y., Berkland, C., Liang, J.-T., Moradi-araghi, A., Christian, T., Needham, R., Hedges, J., Cheng, M., Scully, F., Zornes, D., 2019. Delayed Gelling Agents, US2019/0071598A1. US Patent.

Moradi-Araghi, A., Beardmore, D., Stahl, G., 1988. The application of gels in enhanced oil recovery: theory, polymers and crosslinker systems. In: Stahl, G.A., Schulz, D.N. (Eds.), Water-Soluble Polymers for Petroleum Recovery. Springer, pp. 299–312. https://doi.org/10.1007/978-1-4757-1985-7_21.

Muñoz-Espí, R., Landfester, K., 2020. Low−temperature miniemulsion−based routes for synthesis of metal oxides. Chem. Eur J. 26 (42), 9304–9313. https://doi.org/10.1002/chem.202001246.

Musyanovych, A., Landfester, K., 2014. Polymer micro- and nanocapsules as biological carriers with multifunctional properties. Macromol. Biosci. 14 (4), 458–477. https://doi.org/10.1002/mabi.201300551.

Néstor, M.-M., Kei, N.-P.E., Guadalupe, N.-A.M., Elisa, M.-E.S., Adriana, G.-Q., David, Q.-G., 2011. Preparation and in vitro evaluation of poly (D, L-lactide-co-glycolide) air-filled nanocapsules as a contrast agent for ultrasound imaging. Ultrasonics 51 (7), 839–845. https://doi.org/10.1016/j.ultras.2011.04.003.

Ogolo, N., Olafuyi, O., Onyekonwu, M., 2012. Enhanced oil recovery using nanoparticle. SPE Saudi Arabia Sec. Tech. Symp. Exhibition. https://doi.org/10.1016/j.ptlrs.2021.03.003.

Paiphansiri, U., Tangboriboonrat, P., Landfester, K., 2006a. Polymeric nanocapsules

containing an antiseptic agent obtained by controlled nanoprecipitation onto water-in-oil miniemulsion droplets. Macromol. Biosci. 6 (1), 33–40. https://doi.org/10.1002/mabi.200500178.

Paiphansiri, U., Tangboriboonrat, P., Landfester, K., 2006b. Polymeric nanocapsules containing an antiseptic agent obtained by controlled nanoprecipitation onto water-in-oil miniemulsion droplets. Macromol. Biosci. 6 (1), 33–40. https://doi.org/10.1002/mabi.200500178.

Piñón-Segundo, E., Llera-Rojas, V.G., Leyva-Gómez, G., Urbán-Morlán, Z., Mendoza-Muñoz, N., Quintanar-Guerrero, D., 2018. Chapter 2 - The emulsification-diffusion method to obtain polymeric nanoparticles: two decades of research. In: Grumezescu, A.M. (Ed.), Nanoscale Fabrication, Optimization, Scale-Up and Biological Aspects of Pharmaceutical Nanotechnology. William Andrew Publishing, pp. 51–83. https://doi.org/10.1016/B978-0-12-813629-4.00002-4.

Pu, J., Bai, B., Alhuraishawy, A., Schuman, T., Chen, Y., Sun, X., 2019a. A recrosslinkable preformed particle gel for conformance control in heterogeneous reservoirs containing linear-flow features. SPE J. 24 (4), 1714–1725. https://doi.org/10.2118/191697-PA.

Pu, J., Geng, J., Han, P., Bai, B., 2019b. Preparation and salt-insensitive behavior study of swellable, Cr3+-embedded microgels for water management. J. Mol. Liq. 273, 551–558. https://doi.org/10.1016/j.molliq.2018.10.070.

Reddy, B.R., Eoff, L., Dalrymple, E.D., Black, K., Brown, D., Rietjens, M., 2002. A natural polymer-based crosslinker system for conformance gel systems. SPE J.

8 (2), 99–106. https://doi.org/10.2118/84937-PA.

Seright, R., Brattekas, B., 2021. Water shutoff and conformance improvement: an introduction. Petrol. Sci. 18 (2), 450–478. https://doi.org/10.1007/s12182-021-00546-1.

Sun, X., Suresh, S., Zhao, X., Bai, B., 2018. Effect of supercritical CO_2 on the dehydration of polyacrylamide-based super-absorbent polymer used for water management. Fuel 224, 628–636. https://doi.org/10.1016/j.fuel.2018.03.103.

Sydansk, R.D., Southwell, G.P., 2000. More than 12 years' experience with a successful conformance-control polymer-gel technology. SPE Prod. Facil. 15 (4), 270–278. https://doi.org/10.2118/66558-PA.

Veisi, M., Johnson, S., Peltier, K., Berkland, C., Liang, J.-T., Barati, R., 2018. Application of polyelectrolyte complex nanoparticles to increase the lifetime of poly vinyl sulfonate scale inhibitor. SPE Int. Conf. Exhibition Format. Damage Contr. Proc. https://doi.org/10.2118/189564-MS.

Willhite, G., Pancake, R., 2004. Controlling water production using gel polymer system. SPE/DOE Symp.Improved Oil Recovery. https://doi.org/10.2118/89464-MS.

Yin, W., Liu, H., Yates, M.Z., Du, H., Jiang, F., Guo, L., Krauss, T.D., 2007. Fluorescent quantum dot−polymer nanocomposite particles by emulsification/solvent evaporation. Chem. Mater. 19 (12), 2930−2936. https://doi.org/10.1021/cm070214g.